JOURNAL OF MATERIALS SCIENCE 30 (1995) 69–74

Effect of viscous flow on the thermal residual stresses in a monofilament SiC/borosilicate glass composite

M. BARSOUM, A. ELKIND
Materials Engineering Department, Drexel University, Philadelphia, PA 19104, USA

Residual strains of SiC (SCS-6) single fibres embedded between borosilicate slides were measured by comparing their post-fabricated *in situ* lengths with their original lengths as a function of processing temperature and load in an open die. If cooled without load the residual strains agreed with the values one would expect if the stress-free temperature was taken to be the strain point of the glass. However, if cooled under load, the residual strains were found to be significantly enhanced, and increased linearly with the applied load, but were insensitive to processing temperature. A hydrodynamic model, where glass flow normal to the vertically applied pressure entrains the embedded fibres and results in the enhanced residual strains, is proposed. The implications of these results in calculating thermal residual stresses in viscous media are discussed. At higher applied loads, the fibre edges broke into smaller fragments. The fragment length distribution was measured and analysed using Weibull statistics. Heat treatment of the fibres at 1600 °C for 4 h in vacuum, resulted in approximately a 50% decrease in their strength and critical length as compared to the as-received fibres. The Weibull moduli, however, were not affected by the heat treatment.

1. Introduction

One of the more important considerations in designing ceramic/glass or ceramic/ceramic composites is the thermal expansion mismatch between the reinforcing phase and that of the matrix. For fibre-reinforced ceramic matrix composites, both the radial and axial thermal expansion mismatches are important. If the fibres have a larger coefficient of thermal expansion (CTE) than the matrix, then upon cooling from the processing temperature the matrix will be in axial compression and the fibre/matrix interface will be in tension and will tend to debond. Conversely, if the CTE of the fibres is lower than that of the matrix, the latter will radially clamp down on the fibres upon cooling and an axial residual stress in the matrix will ensue. In either case degradation of the mechanical properties of the composites can ensue.

Several experimental techniques have been used to measure the state of residual stresses in composite materials. Photoelastic measurements are well established for glasses [1], and other transparent materials. More recently, embedded optical fibres have been used to measure residual stresses and to detect damage in composites [2]. X-ray and neutron diffraction peak shifts have also been used to measure the surface stress state of materials [3–5]. Raman spectroscopy has also been used by Galiotis *et al.* [6, 7] and others [8, 9] to determine the strain in monofilament composites. The advantage of this technique is that it can be used to map the strain along the fibre length. Virkar *et al.* [10] used strain gauges for measuring residual stress profiles. Most of these techniques, however, are indirect and require independent calibration procedures to determine the actual strains.

In addition to the state of residual stresses in composites, another important composite characteristic is the work of failure and ultimate tensile strength. The existing theories predict complicated dependencies of the work of pullout and composite ultimate tensile stress on the Weibull modulus of the fibres, m, their average strength, σ_0, the frictional sliding resistance between fibre and matrix, τ, and the fibre radius, ρ [11–13]. Recently, Curtin [12] has shown that the characteristic length of fibre fragments, δ_c, was a key indicator of uniaxial tensile composite performance. δ_c, in turn, was expressed as [12]

$$\delta_c = \left[\frac{\sigma_0 \rho (2\lambda)^{1/m}}{\tau}\right]^{\frac{m}{m+1}} \quad (1)$$

where 2λ is the fibre gauge length.

In polymer matrix composites, δ_c is usually measured by embedding the fibres in a large strain-to-failure matrix and loading the latter to the point that the fibres fragment [14, 15]. While this technique is fairly straightforward, it has not been applied to ceramic fibres because, for the most part, their strains-to-failure are higher than those of most ceramic matrices.

Experimentally, the only technique, that we are aware of, that has been used to measure δ_c of ceramic fibres entails measuring the pullout length distribution of the fibres after loading of composite samples to

0022–2461

failure [16]. This technique, however, only measures the pullout or critical lengths of the fibres *after* processing of the composites, and has only been applied to Nicalon-containing composites. To date, no data have been reported for the critical lengths of SCS–6 SiC monofilaments.

In this paper, a novel technique for measuring the residual thermal strains in monofilament composites is described. The technique is based on comparing the post-processing *in situ* and initial lengths of fibres that had been embedded between two glass plates as a function of processing load and temperature. The transparency of the glass allows for the *in situ* measurements of the fibre lengths. As discussed below, a further advantage of this technique is that it can also be used to measure the critical lengths of ceramic fibres. With the simultaneous application of heat and pressure, the glass behaves as a large strain-to failure matrix and results in the fragmentation of the fibres.

The objective of this study was two-fold. The first was to employ this technique to measure the thermal residual strains developed in SiC monofilaments embedded between borosilicate glass slides as a function of processing temperature and applied loads in order to understand better the role of each on these residual strains. The second was to measure the critical lengths of SCS–6 SiC monofilaments.

2. Experimental procedure

The system used was a model system where large diameter (140 μm) SiC (SiC Filament grade SCS-6, Textron Specialty Materials, Textron Inc., Lowell, MA) monofilaments were embedded between borosilicate glass (7740, Corning, NY) slides. This system was chosen for two reasons: (i) it is reasonably well characterized [17–21] and, (ii) the large diameter of the fibres and their strengths allowed for ease of handling.

The thermal residual stresses at room temperature were measured as follows. Short strands of SiC SCS-6 fibre were cut and their lengths were carefully measured using a machinists microscope (Gaertner Scientific Corp., Chicago, IL) with a resolution estimated to be $\pm$ 2 μm. Single-fibre strands (1.5–2.5 cm long) were placed between two borosilicate slides (2–3 cm long, 0.5–1.5 cm wide and 0.15 cm thick), heated in air at 10° C min^{-1} to various temperatures under various dead loads corresponding to stresses between 0.05 and 0.5 MPa, in an open die. A cross-section of the fibre/matrix assembly prior to processing is shown in Fig. 1a. Each sandwich contained only one fibre and a picture of the final fibre/matrix configuration after processing is shown in Fig. 2. No special procedures were taken to ensure that the plates were parallel; however, the uniformity in thickness of the post-fabricated specimen was taken as evidence that the plates remained parallel throughout the processing.

The samples were typically heated to the processing temperature, held at temperature for 30 min and then furnace cooled under the dead load (cooling rate was approximately 5° C min^{-1}). In a few runs, however, in which the dead load corresponded to 0.05 MPa, the load was removed prior to furnace cooling. These data are presented on the *y*-axis in Fig. 3. Two temperatures were investigated, 700 and 800 °C. At temperatures higher than 800 °C bubbles were observed at the glass–fibre interface (Fig. 4), whereas at temperatures lower than 700 °C the glass slides did not adhere to each other. After cooling to room temperature, the samples were placed in the machinists microscope and the embedded fibre lengths were remeasured *in situ* while still sandwiched between the two glass

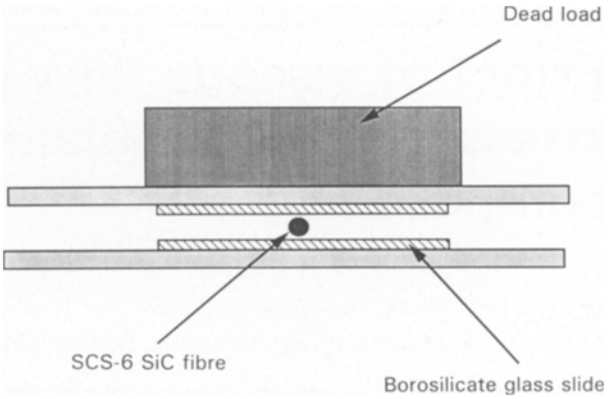

Figure 1 Schematic drawing of assembly during processing.

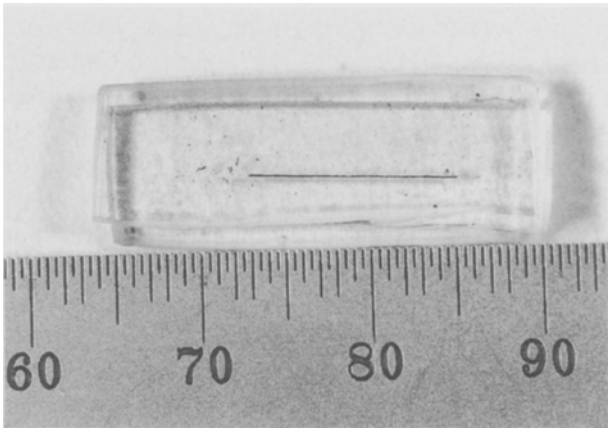

Figure 2 Picture of the fibre/matrix assembly. This sample was processed at 700 °C under a load of 0.5 MPa which resulted in fragmentation of the fibre edges. When processed at loads < 0.2 MPa, the fibres remained intact.

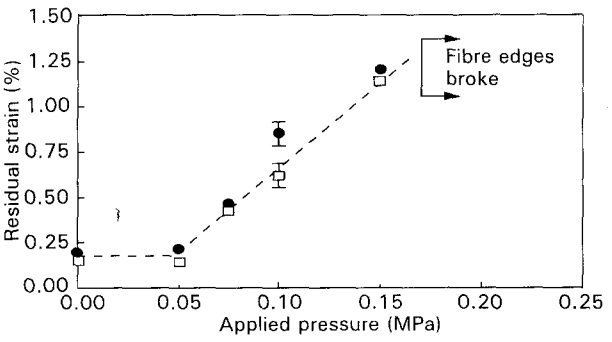

Figure 3 Functional dependence of residual strain on applied load and temperature during processing. At loads greater than ≈ 0.2 MPa the fibres fragmented at the edges. (□) 700 °C, (●) 800 °C.

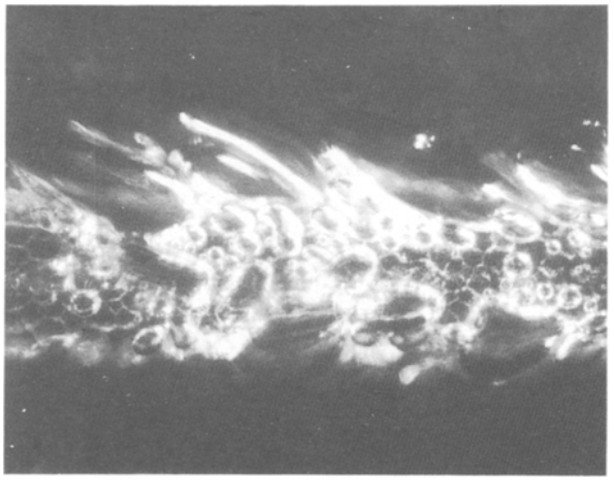

Figure 4 Bubble formation at the glass/fibre interface for fibres processed at 850 °C.

slides. The dependence of the residual strains on temperature and applied load during processing is plotted in Fig. 3. Each point represents the average of at least three independent measurements.

To ensure that parallax effects were negligible, the embedded lengths of a set of fibres were measured, after which the matrix was cut flush with the fibre edges and fibre lengths were remeasured. No significant difference between the two sets of data was observed. Furthermore, because the matrix was transparent, fibre curvature, if present, was easily taken into account.

For applied stresses greater than 0.15–0.2 MPa, the fibre edges broke into smaller fragments as shown in Fig. 2. The lengths of these fragments were measured and analysed using Weibull statistics. It is important to note at this point that fragmentation of the fibres occurred only when the assembly was furnace cooled under load. If the load was removed at the annealing temperature and the samples were furnace cooled without load, no fragmentation was observed even with loads corresponding to 0.5 MPa. This implies, as discussed later, that the strain develops upon cooling of the samples and not at the processing temperature.

In order to examine the influence of fibre strength on the critical length, a number of fibres were heated in a vacuum hot press (10^{-4} torr; 1 torr = 133.322 Pa) for 4 h at 1600 °C and embedded between the glass slides under an applied stress of 0.5 MPa. The critical length of the fibres was measured and the strength of these heat-treated fibres was measured independently.

The tensile strengths of the fibres at room temperature were measured by placing the fibres in a paper mounting frame and epoxied in place leaving 50 mm as gauge length. Fibre specimens were pulled to failure using an Instron (Instron, Canton, MA) at a constant crosshead speed of 0.05 mm min^{-1}. An average of at least three samples were tested for each heat-treatment condition.

3. Results and discussion

The functional dependence of the residual strains on the processing temperatures and applied loads is shown in Fig. 3. In all cases the strains were tensile and increased linearly with increasing applied load. The differences between the residual thermal strains for samples processed at 800 and 700 °C, however, were negligible and within experimental scatter. At strains greater than $\approx 1.25\%$ the fibre edges broke into smaller fragments (Fig. 2).

These results are quite intriguing because with the notable exception of the samples that were cooled without load and/or at low loads, they are significantly higher than one would theoretically predict based on the simple expression for thermal residual strain:

$$\varepsilon_{th} = \Delta\alpha\,\Delta T \tag{2}$$

where $\Delta\alpha$ is the difference between thermal expansion coefficients of the fibres and matrix, and ΔT the difference between the strain point of the matrix and room temperature. In a previous paper, the CTEs of the SiC monofilaments and the borosilicate matrix were measured to be $6.5 \pm 0.5 \times 10^{-6}$ and $3.1 \times 10^{-6}\,°C^{-1}$, respectively [21]. The strain point of the matrix is 525 °C, thus according to Equation 2, the corresponding residual strain is 0.0016 ± 0.0003. This value is in good agreement with the measured residual strains for samples that were cooled without loads, or with loads of < 0.05 MPa, namely 0.0014 ± 0.0003, which. This confirms not only the validity of the residual strain measurements but also the value of $6.5 \pm 0.5 \times 10^{-6}\,°C^{-1}$ for the CTE of the fibres measured previously [21].

Fig. 3 clearly shows that the residual strains increase linearly with applied load and are at least a factor of four greater than what one would predict based on Equation 2. It is important to note that even if one assumes that the thermal expansion of the glass was zero and that perfect bonding existed between the fibres and matrices, the calculated residual strain of ≈ 0.0034 is still significantly lower than the ones observed. It thus appears that another mechanism is responsible for this intriguing phenomenon that to the best of our knowledge has not been reported before. It is proposed here that the hydrodynamic flow of the viscous matrix normal to the applied load entrains the embedded fibres resulting in the observed strain. A model is proposed below to quantify the effect.

By assuming the total axial residual strain, ε_{total}, in the fibre is the sum of the thermal residual strain, $\varepsilon_{th} = \Delta\alpha\,\Delta T$, and that due to viscous flow, ε_v, it follows that

$$\begin{aligned} \varepsilon_v &= \varepsilon_{total} - \varepsilon_{th} \\ &= \varepsilon_{total} - \Delta\alpha\,\Delta T \end{aligned} \tag{3}$$

Locally, ε_v, in turn, is related to the shear stress in the fibre, τ_v, according to

$$\tau_v = \varepsilon_v E_f \rho / 4\lambda \tag{4}$$

where E_f is the Young's modulus of the fibres.

The viscous flow of the glass matrix can be modelled as a one-dimensional squeezing flow between two parallel plates initially separated by a distance $2h$, under a constant pressure, P_{app}, applied to each plate. The coordinate system is shown in Fig. 5a,

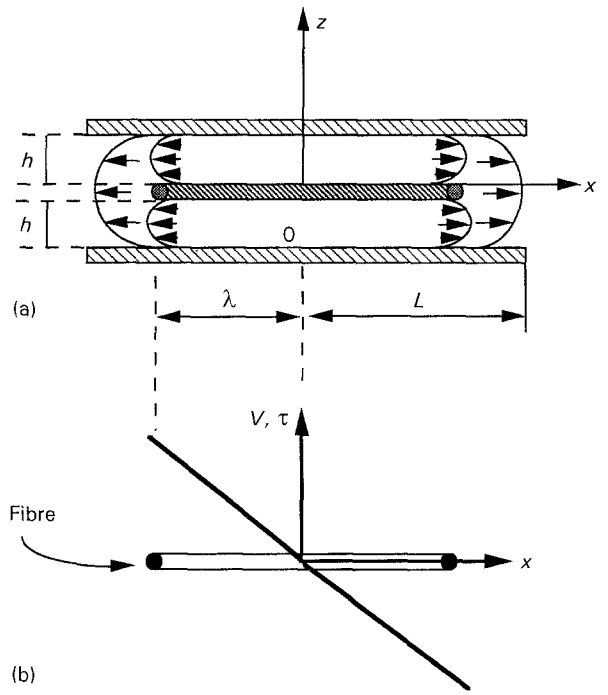

Figure 5 (a) Schematic drawing of fibre and glass slide assembly. The origin was chosen as shown. The curved surfaces schematically indicate the perturbation in the velocity as a result of the presence of the fibre. (b) Shear and velocity distribution along the fibre length. Both are zero at the centre of the fibre and reach a maximum at the fibre edges.

and given the symmetry of the problem, only the range $z = 0$ or $z = h$ will be considered, where z is the vertical coordinate.

To solve the problem exactly the pressure distribution at the fibre surface has to be known, which is non-trivial since a simple analytical expression does not exist. Thus we make the simplifying assumption that: the pressure distribution in the glass matrix is unperturbed by the presence of the fibre. The validity of this assumption and its implications is discussed below.

The pressure distribution in the glass slides is non-uniform and is given by [22]

$$P(x) - P_{atm} = -12\,\mu_m\left(\frac{dh}{dt}\right)\frac{1}{h^3}\left(\frac{x^2}{2} - \frac{L^2}{2}\right) \quad (5)$$

where $2L$, μ_m, P_{atm}, are the length of the glass slide, its viscosity and atmospheric pressure, respectively. By carrying out a simple force balance, it can be shown that $P(x)$ is related to the applied pressure, P_{app}, by

$$P_{app} = \frac{4\mu_m L^2}{h^3}\left(\frac{dh}{dt}\right) \quad (6)$$

To estimate the shear forces acting on the fibre surface as a result of matrix flow, the velocity gradients at that surface have to be known. Assuming the fibre acts as a flat plate, the functional dependence of the flow velocity in one x direction on z and x is given by [22]

$$V_x = -6x\frac{dh}{dt}\frac{1}{h^3}(z^2 - hz) \quad (7)$$

The corresponding shear stress at the fibre surface, τ_m, is given by [22]

$$\tau_m = -\mu_f\left(\frac{dV_x}{dz}\right)_{z=0} \quad (8)$$

where μ_f is the viscosity of the matrix at the fibre surface. Eliminating dh/dt, from Equations 6–8 one obtains

$$\tau_m = \frac{3}{2}\frac{hx\mu_f}{L^2\mu_m}P_{app} \quad (9)$$

The velocity and shear stress distribution are shown in Fig. 5b. The shear stress is maximum at the fibre edges and zero at its centre. Further, assuming the shear stresses at the fibre surface and that in the matrix are related by

$$\tau_v = k\tau_m \quad (10)$$

where k is the coefficient of friction, and combining Equations 3, 4, 9 and 10, the relation between ε_v, and P_{app}, is given by

$$\begin{aligned}\varepsilon_v &= \frac{\Delta\lambda}{\lambda} \\ &= \int_0^{\lambda}\frac{4\tau_v}{E_f\rho\mu_m}dx \\ &= \frac{3kh\lambda^2\mu_f}{L^2E_f\rho\mu_m}P_{app}\end{aligned} \quad (11)$$

where we assumed that the fibre is centred with respect to the glass slide. Equation 11 predicts that ε_v should increase linearly with applied load, which is confirmed by the experimental results shown in Fig. 3. It should be noted that in Fig. 3, ε_{total} rather than ε_v is potted. However, because ε_{th} is constant, this simply shifts the dotted line in Fig. 3 downwards by ε_{th}. Why the line does not go through the origin is not clear at this point.

Thus, qualitatively, the model captures the essence of the results quite well. Quantitatively, however, if one assumes that μ_f and μ_m are equal, then the model is less accurate. For example, assuming $\mu_f = \mu_m$, $k = 1$ and taking $\lambda = 0.8\,L$, $h = 1.5$ mm, $E_f = 400$ GPa [23, 24] and $\rho = 70$ μm, the theoretical slope (Equation 11) is calculated to be 1×10^{-4} MPa^{-1}. However, the experimental slope calculated from Fig. 3 is 0.1 MPa^{-1}. In other words, the measured axial residual strains are approximately 1000 times higher than one would predict based on this viscous drag model.

The exact reason for the discrepancy is not clear, but several possibilities exist. Clearly the model is limited in that it assumes steady state and isothermal conditions. As noted above, the strains develop upon cooling, and therefore reconciling the model predictions with the experimental results would require a detailed knowledge of the heat transfer out to the sample, the exact temperature dependence of μ_f and μ_m, and the effect any reaction between the fibre and matrix on μ_m would have. Another simplifying assumption that was made in deriving Equation 11 was that the pressure distribution in the glass matrix was unperturbed by the presence of the fibres. This assumption clearly underestimates the pressure at the

fibre surface – the fibre does constitute an inhomogeneity and stress concentrations at the fibre surface are likely. Given that in each case the simplifying assumptions would tend to underestimate μ_f/μ_m, it is not inconceivable that sometime during cooling that ratio could reach 1000.

Despite this discrepancy we believe that this model captures the physics of the situation for the following simple reason: had the ends of the fibre not been dragged by the flowing glass during cooling, then the maximum possible strain that could have been developed in the fibre would be:

$$\varepsilon = (6.5 \times 10^{-6} - 0)(800 - 25) = 0.005 \quad (12)$$

which clearly cannot account for the observed values. Said otherwise, if the maximum lengths of the fibres, reached at the processing temperature had not increased further during cooling, it would be impossible to account for the observed strains.

As noted earlier, at a processing temperature higher than 800 °C bubbles formed at the glass/fibre interface (Fig. 4). These bubbles, in turn, resulted in total debonding and loss of adhesion, i.e. $k = 0$, between fibres and matrix. Consequently, the residual strains for these samples were negligibly small. Bubble formation is believed to have occurred as a result of reaction between the outermost carbon sheath surrounding the fibres and oxygen, probably forming CO and CO_2.

3.1. Critical lengths

For applied stresses greater than ≈ 0.15 MPa, the fibre ends fragmented (Fig. 2). The lengths of these fragments were measured and plotted using Weibull statistics. The results, for two different loads, 0.4 and 0.5 MPa processed at 700 °C, are plotted in Fig. 6 (lower curve). The average lengths of the fibre fragments were almost identical, 0.37 mm at 0.4 MPa and 0.36 mm at 0.5 MPa. Furthermore, the Weibull moduli for both samples were nearly equal. It is interesting to note that while the average lengths of the fragments were identical, the number of fragments observed under the 0.5 MPa load were significantly greater than at 0.4 MPa, as one would expect.

The Weibull distribution for the fibres that were heat treated at 1600 °C for 4 h is also shown in Fig. 6. The average lengths of the fibre fragments, at 0.19 mm, was about half that of the as-received fibres, but their Weibull modulus ($m = 2.76$) did not change significantly. As noted above, the ultimate tensile strength of the heat-treated fibres were measured and found to be 1.96 GPa, which is about half the as-received strength reported to be 3.7 GPa [23, 24]. Given this information, the validity of Equation 1 can now be verified. Because λ, ρ and τ are identical for both the as-received and heat-treated fibres it follows that

$$\delta_{c1}/\delta_{c2} = (\sigma_{c1}/\sigma_{c2})^{m/m+1} \quad (13)$$

where 1 and 2 represent the as-received and heat-treated fibres simultaneously. m calculated from Equation 13 is 2, which is in reasonably good agreement with the values of 2.4 and 2.7 measured from the Weibull plots (Fig. 6), directly verifying the validity of Equation 1.

The failure strain of SCS-6 monofilaments has been reported to be approximately 1%. This value is in good agreement with the point at which fibre breakage was first observed in our work (Fig. 3) and is

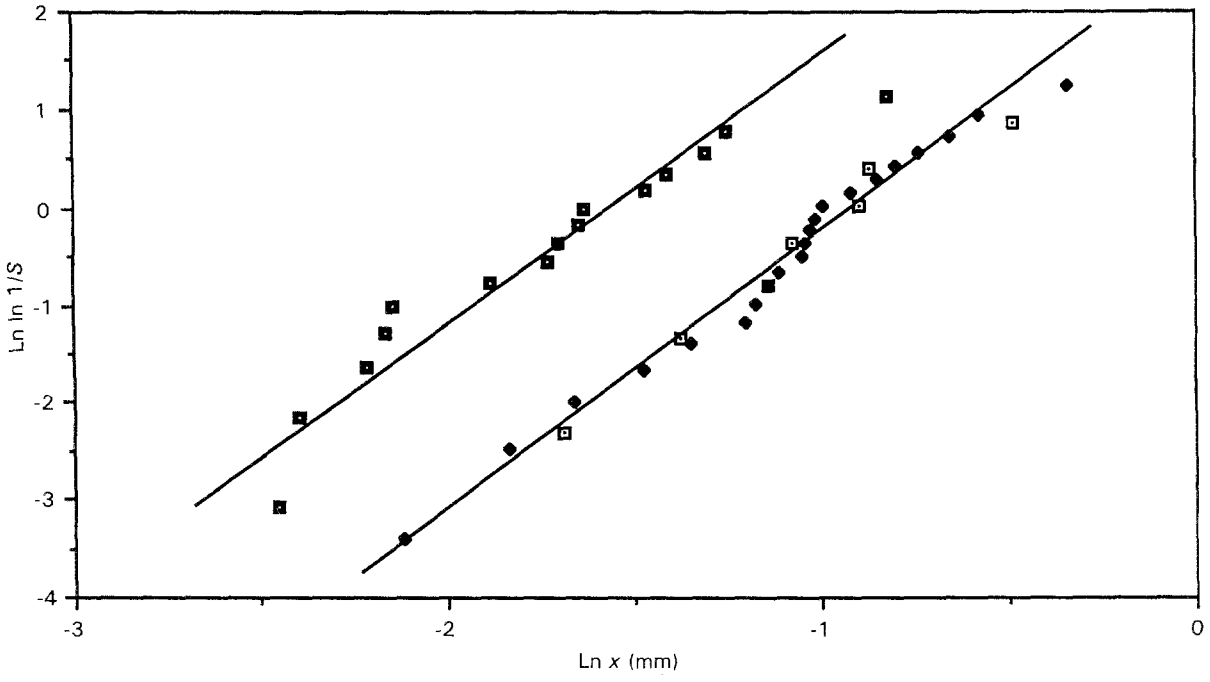

Figure 6 Weibull distribution of post-processing length of fibre fragments for as-received and heat treated (1600 °C for 4 h) fibres. All tests were carried out at 700 °C. The as-received fibres were tested under two different loads: (□) 0.4 MPa, (◆) 0.5 MPa. The Weibull modulus remained unchanged and the number of fragments increases as the applied load increased. (■) Heat treatment of the fibres under 0.5 MPa pressure shifted the distribution to lower lengths but did not significantly alter the Weibull modulus.

a further independent confirmation of the validity of this technique for measuring residual strains. Another point that confirms the general validity of the model suggested above is the fact that the fibres broke at the edges rather than uniformly along their entire length. Had the shear stress distribution been uniform, rather than as shown in Fig. 5b, the fibres would have fragmented uniformly along their length.

From a practical point of view the results shown here indicate that the state of residual stress in composites could be quite large, if the latter are processed in open dies or in the situation where matrix flow is allowed to occur.

4. Conclusions

The axial thermal residual stresses developed in 140 μm SiC monofilaments embedded between borosilicate glass slides were measured by comparing the *in situ* lengths of the embedded fibres to their original lengths as a function of processing temperature and load in open dies and the following conclusions were reached.

1. The residual strains in the presence of applied loads were significantly enhanced, as a result of normal applied loads during processing.
2. The enhancement in strain increased linearly with applied load and was an insensitive function of processing temperature.
3. A model in which the entrainment of the fibres in the flow of the glass matrix as a result of the applied pressure, results in the excess strain was developed.
4. The critical lengths of SiC fibres, both heat treated and as-received, were also measured *in situ* and statistically analysed using Weibull statistics. Heat treatment of the fibres at 1600 °C for 4 h resulted in a 50% decrease in both strength and critical length as compared to the as-received fibres. The Weibull moduli, however, were not affected by the heat treatment.

Acknowledgements

We are grateful to Drs Young Cho and Chun Lau of the Department of Mechanical Engineering at Drexel University for valuable discussions and for carefully going through the manuscript.

References

1. A. J. MONACK and E. E. BEETON, *Glass Ind.* **20** (4) (1939) 127.
2. B. HOFER, *Composites* **18** (1987) 309.
3. F. F. LANGE, M. R. JAMES and D. J. GREEN, *J. Am. Ceram. Soc.* **66** (1983) C16.
4. A. J. ALLEN, M. T. HUTCHINGS, C. G. WINDSOR and C. ANDREANI, (NDT International, 1981) p. 249.
5. I. C. NOYAN and J. B. COHEN, Residual Stress. (Springer Verlag, New York, 1987).
6. C. GALIOTIS, R. J. YOUNG, P. H. J. YEUNG and D. N. BATCHELDER, *J. Mater. Sci.* **19** (1984) 3640.
7. C. GALIOTIS and D. N. BATCHELDER, *J. Mater. Sci. Lett.* **7** (1988) 545.
8. L. S. SCHADLER, C. LAIRD, N. MELANITIS, C. GALIOTIS and J. C. FIGUEROA, *J. Mater. Sci.* **19** (1984) 3640.
9. C. GALIOTIS, R. J. YOUNG, P. H. J. YEUNG and D. N. BATCHELDER, *ibid.* **27** (1992) 1663.
10. A. V. VIRKAR, J. L. HUANG and R. A. CUTLER, *J. Am. Ceram. Soc.* **70** (3) (1987) 164.
11. M. SUTCU, *Acta Metall.* **37** (1989) 651.
12. W. A. CURTIN, *J. Am. Ceram. Soc.* **74** (1991) 2837.
13. M. D. THOULESS and A. G. EVANS, *Acta Metall.* **36** (1988) 517.
14. H. F. WU, G. BIRESAW and J. T. LAEMMLE, *Polym. Compos.* **12** (1991) 281.
15. A. N. NETRAVALI, R. B. HENSTENBURG, S. L. PHOENIX and P. SCHWARTZ, *ibid.* **10** (1989) 226.
16. M. D. THOULESS, O. SBAIBERO, L. S. SIGL and A. G. EVANS, *J. Am. Ceram. Soc.* **72** (1989) 525.
17. P. JERO, R. KERANS and T. PARTHASARATHY, *ibid.* **74** (1991) 2793.
18. R. W. GOETTLER and K. T. FABER, *Compos. Sci. Technol.* **37** (1989) 129.
19. J. BRIGHT, S. DANCHAIVIJIT and D. SHETTY, *J. Am. Ceram. Soc.* **74** (1991) 115.
20. M. BARSOUM, P. KANGUTKAR and A. S. D. WANG, *Compos. Sci. Technol.* **44** (1992) 257.
21. A. ELKIND, M. BARSOUM and P. KANGUTKAR, *J. Am. Ceram. Soc.* **75** (1992) 2871.
22. L. D. LANDAU and L. M. LIFSHITZ, "Fluid Mechanics" (Pergamon, London, 1959).
23. K. M. PREWO, J. J. BRENNAN and G. K. LAYDEN, *Ceram. Bull.* **65** (1986) 305.
24. E. FITZER and G. GADOW, *ibid.* **65** (1986) 326.

Received 7 January
and accepted 9 June 1994